Australian Earthquake Engineering Society
2024 National Conference, 21-23 November 2024
Adelaide, South Australia

Broadband Ground Motion Simulation for the 6 February 2023 Mw 7.8 Pazarcık Earthquake, Kahramanmaraş, Türkiye: Methodology and Preliminary Results

Yuxiang Tang[1], Hiroe Miyake[2] and P. Martin Mai[3]

1. *School of Geography, Earth and Atmospheric Sciences, The University of Melbourne, Parkville, Australia, VIC3010.*

2. Earthquake Research Institute, University of Tokyo, Tokyo, Japan, 113-0032.

3. Division of Physical Sciences and Engineering, King Abdullah University of Science and Technology, Thuwal, Saudi Arabia, 23955.

Correspond to: yuxiang.tang@unimelb.edu.au

Abstract

The Mw 7.8 Pazarcık earthquake of February 6, 2023, had catastrophic impact on south-central Türkiye and northwestern Syria, resulting in over 50,000 casualties and extensive destruction. To better understand the earthquake's rupture properties and seismic-wave propagation, we conducted broadband ground motion simulations using a state-of-the-art approach that integrates various physical parameters. The rupture model, based on Mai et al. (2023), was derived from kinematic inversion of teleseismic and geodetic data, while distance- and frequency-dependent attenuation parameters were calibrated using strong motion recordings (Tang et al., 2024). This study outlines the simulation methodology and presents preliminary results for 19 close-distance, pulse-like waveforms. Simulations were performed using an enhanced version of GMSS (Tang, 2022a, 2022b), which integrates low-frequency physics-based simulations (< ~1.0 Hz) with high-frequency stochastic simulations (> ~1.0 Hz). Key improvements in our approach include the correlation between hypocenter location and slip distribution (Mai et al., 2005), direct corner-frequency calculations based on rise time, and incorporation of high-frequency radiation patterns derived from dynamic rupture modeling. These preliminary results and future studies aim to refine ground motion characterizations, supporting seismic hazard assessment in affected regions.

Keywords: broadband simulation; source characteristics; slip model; finite-fault modelling.

1 Introduction

The two devastating earthquakes that struck south-central Türkiye and northwestern Syria on 6 February 2023 serve as a stark reminder that earthquakes can neither be predicted nor prevented. Also, hazard assessment alone is insufficient if risk mitigation procedures are ignored or circumvented. These earthquakes were the deadliest in Türkiye in centuries and resulted in widespread destruction across both Türkiye and Syria. The first earthquake, a

magnitude Mw 7.8 event, was followed just nine hours later by a second Mw 7.6 earthquake, making this sequence unprecedented in recent history for its rapid succession of large-magnitude events on nearby faults. These earthquakes were the deadliest in Türkiye in centuries, resulting in a significant loss of life and widespread destruction across both Türkiye and Syria. The first event nucleated east of the East Anatolian Fault (EAF), a major left-lateral strike-slip fault marking the boundary between the Anatolian and Arabian plates (Pousse-Beltran et al., 2020). The second event occurred on the Sürgü Fault, a lesser-known, east-west trending fault approximately 90 km north of the EAF.

The EAF, along with the North Anatolian Fault (NAF), accommodates the westward extrusion of the Anatolian plate as resulting from the Arabia-Eurasia collision. Over its 500 km length, the EAF has an estimated slip rate of approximately 10 mm/yr (Aktug et al., 2016), but in recent decades, it has been less seismically active than its northern counterpart, the NAF, which has produced numerous large earthquakes, including the destructive 1939 Erzincan Mw 7.8 event and the 1999 Mw 7.6 Izmit earthquake (Barka, 1996). In contrast, the EAF has seen only moderate-sized events over the past century, such as the 2020 Mw 6.8 Elazığ earthquake (Bayik et al., 2020).

The 2023 earthquakes highlight several important aspects of seismic hazard in the region, especially the occurrence of large-magnitude continental strike-slip events. Prior to 2023, only a handful of strike-slip earthquakes worldwide have exceeded Mw 7.5, such as the 2002 Mw 7.9 Denali earthquake and the 2016 Mw 7.8 Kaikoura earthquake. Each of these events has revealed complex rupture behaviors due to fault geometry, and the 2023 earthquakes are no exception. Real-time aftershock locations suggest that the rupture length for the Mw 7.8 event extended approximately 350 km along the EAF, while the Mw 7.6 rupture covered around 170 km along the Sürgü Fault.

In terms of ground shaking, the two earthquakes generated ground motions that exceeded the expected values for a 475-year return period across a significant portion of the affected area. Preliminary analysis of the ground motions from the Mw 7.8 earthquake, such as the studies by Bindi et al. (2023) and Mai et al. (2023), indicates that the ground motion intensities far exceeded previous estimates based on regional seismic hazard models (Şeşetyan et al., 2018). The events also underline the necessity of more robust ground motion models that accurately capture the effects of large-magnitude earthquakes, particularly at close distances.

Although the availability of a large amount of well-recorded data enables a detailed investigation of ground motion properties, simulation-based data that encode earthquake physics with well-calibrated parameters are essential for facilitating local seismic hazard and risk analysis. To address this need, we simulated ground motions for the event using the latest version of the GMSS3.0 code, allowing us to examine the source characteristics and other ground shaking properties.

2 Methodology

2.1 Deterministic physics-based simulation

Similar to existing methodologies, our approach to broadband ground motion simulation integrates two primary components: a low-frequency, deterministic, physics-based component (< ~1.0 Hz) and a high-frequency stochastic component (> ~1.0 Hz) (Miyake et al., 2003; Mai et al., 2010; Graves and Pitarka, 2010). For both components, the source rupture model is generated using the GMSS3.0 code, which incorporates a "realistic" slip distribution model (Mai and Beroza, 2002) and a pseudo-dynamic model (Guatteri et al., 2005), or alternatively, it is derived from kinematic finite fault inversions (Mai and Thingbaijam, 2014). Fig. 1 presents an example of a slip model and the corresponding kinematic source parameters as generated by GMSS3.0.

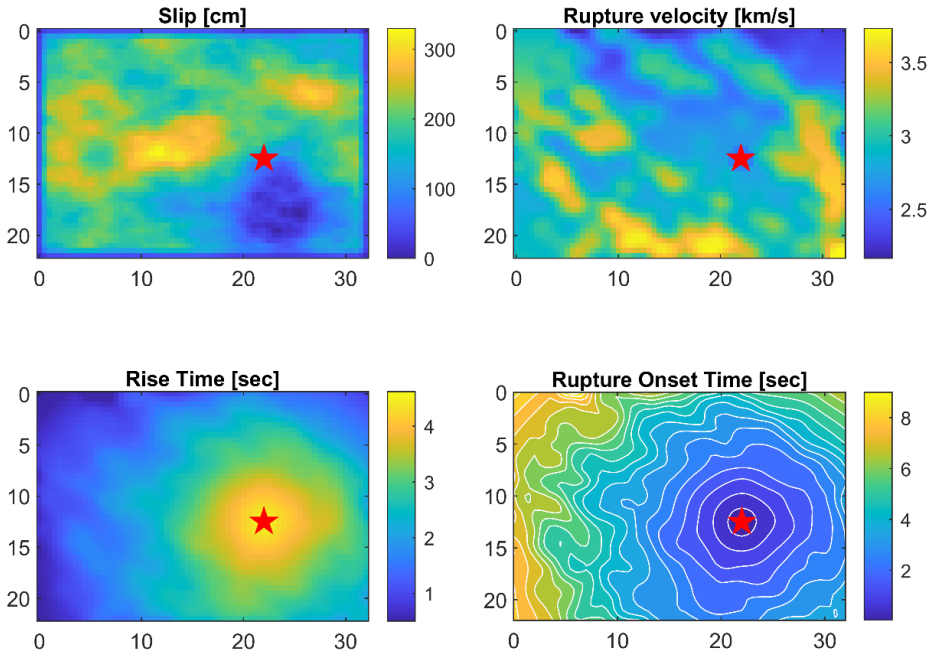

Figure 1. Example slip model and kinematic source parameters generated from GMSS3.0.

In the deterministic simulation, the time series is generated through the convolution of a slip rate (source time) function with the Green's function (Aki and Richards, 1980). GMSS3.0 provides various options for slip rate functions, including the modified Yoffe function (Tinti et al., 2005). For the Green's function, we employ the frequency-wavenumber integration (F-K) method (Zhu and Rivera, 2002), an efficient approach for solving the elastodynamic and elastostatic problems of point sources in multi-layered media by utilizing a re-derived Thompson-Haskell propagator matrix (Thompson, 1950; Haskell, 1953, 1964).

Compared to other methods—such as finite difference, spectral element, or finite element methods—the F-K method offers three main advantages: (i) unlike other methods, which compute the entire wave field, the F-K method computes only the Green's function for specific target points, significantly reducing computational costs; (ii) it requires no complex meshing prior to computation, relying solely on a layered velocity model as input; and (iii) the computed Green's function can be reused across multiple simulations without requiring recalculation.

The F-K method involves a two-step integration process: wavenumber ('K') integration and frequency ('F') integration. The wavenumber integration uses kernels derived from the Thompson-Haskell propagator matrix and multiple Bessel functions, while smoothing is achieved by incorporating attenuation parameters (Q) into the velocity model. The frequency integration is then accomplished via an inverse Fourier transform.

To streamline and integrate the computational process, we developed a MATLAB-based F-K code, which has been incorporated into GMSS3.0. For verification and validation, we conducted a comprehensive comparison with the original F-K code (written in Fortran and C). Figs. 2 and 3 illustrate these comparisons for a sample test case provided by the original F-K code (version 3.4). Specifically, we compared the calculated Green's function over distances ranging from 5 to 300 km (component 0) (Fig. 2) and examined eight components for an epicentral distance of 20 km (Fig. 3) for a double-couple point source.

As shown in Figs. 2 and 3, the MATLAB-based code results closely match those of the original code in terms of amplitude and arrival times, achieving a reasonable level of accuracy.

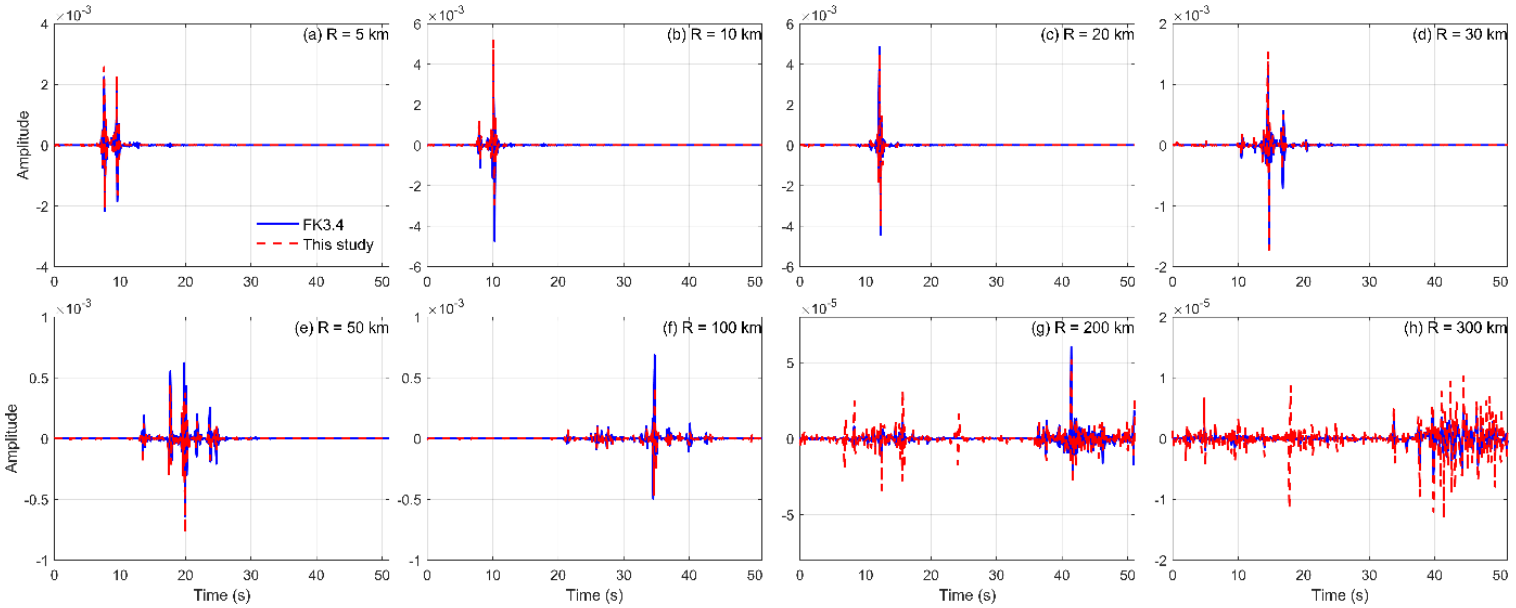

Figure 2. Comparison between our code with original FK code: for component 0 with distance ranging from 5 to 300 km. The source type is set as double couple source, with focal depth of 15 km. The velocity model is adopted from the sample text in the original FK code.

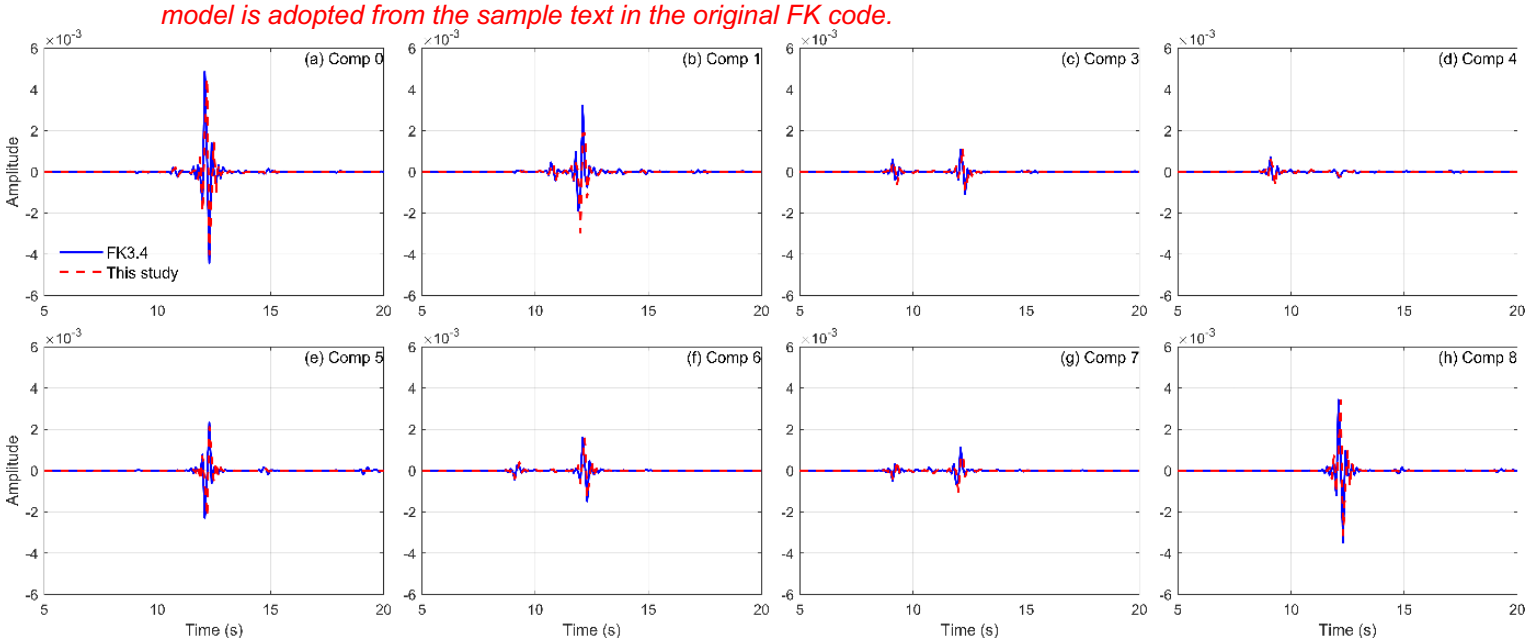

Figure 3. Comparison between our code with original FK code: for 8 components at distance of 20 km. The source type is set as double couple source, with focal depth of 15 km. The velocity model is adopted from the sample text in the original FK code.

Figs. 4-6 present examples of slip rate function, Green's function, and the convolution results, respectively.

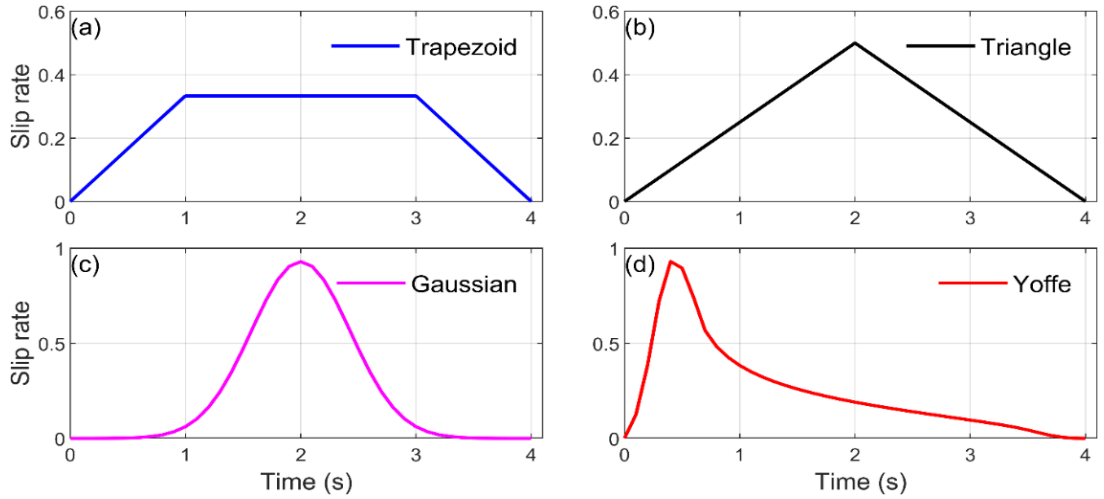

Figure 4. Example slip rate functions contained in GMSS3.0. The rise time is set as 4.0 s in the figure, for all cases.

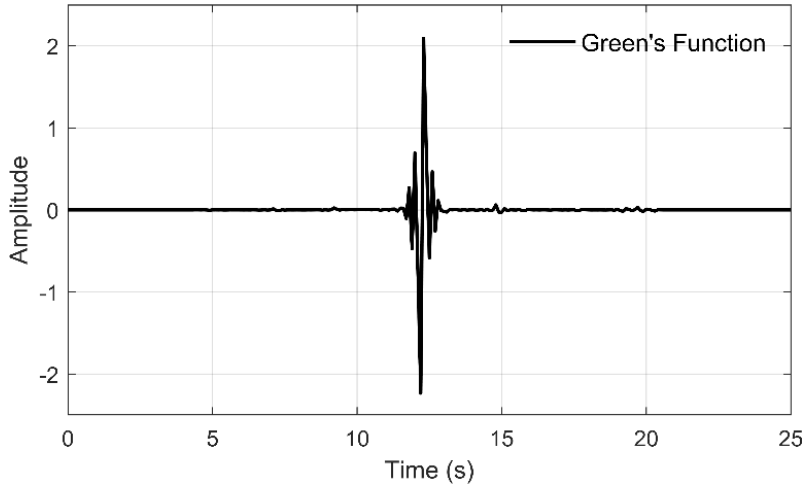

Figure 5. Example Green's function calculated from the FK method, at 20 km, for vertical component.

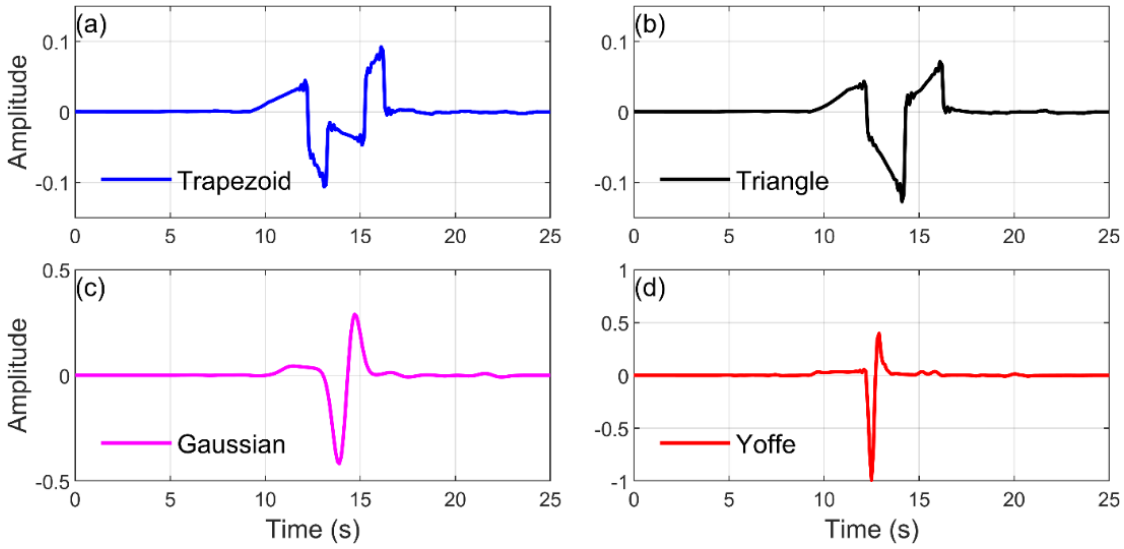

Figure 6. Synthetic time series from the convolution of slip rate functions and the Green's function, for vertical component, at 20 km.

2.2 High-frequency stochastic simulation

For the high-frequency stochastic simulation, we introduce three major improvements over existing methodologies (Motazedian and Atkinson, 2005; Boore, 2009; Tang, 2022a; 2022b).

First, instead of randomly assigning hypocenter locations, we use the methodology proposed by Mai et al. (2005), which correlates hypocenter location with slip distribution. Second, rather than relying on a dynamic corner frequency assumption where corner frequency is inversely proportional to the cumulative ruptured area on the fault, we calculate the corner frequency directly from the rise time, either obtained from kinematic inversion analysis or our pseudo-dynamic modeling. Third, in contrast to using an average radiation pattern value, we incorporate a high-frequency radiation pattern derived from dynamic rupture modeling (Pulido and Dalguer, 2009) into our simulations. These improvements aim to make our simulations more physics-based, while remaining applicable for engineering purposes.

We combine the low-frequency synthetic waveforms and high-frequency seismograms in the frequency domain using a specified merging frequency (e.g., 1.0 Hz). Fig. 7 illustrates an example of the resulting broadband simulation, shown in both the time and frequency domains.

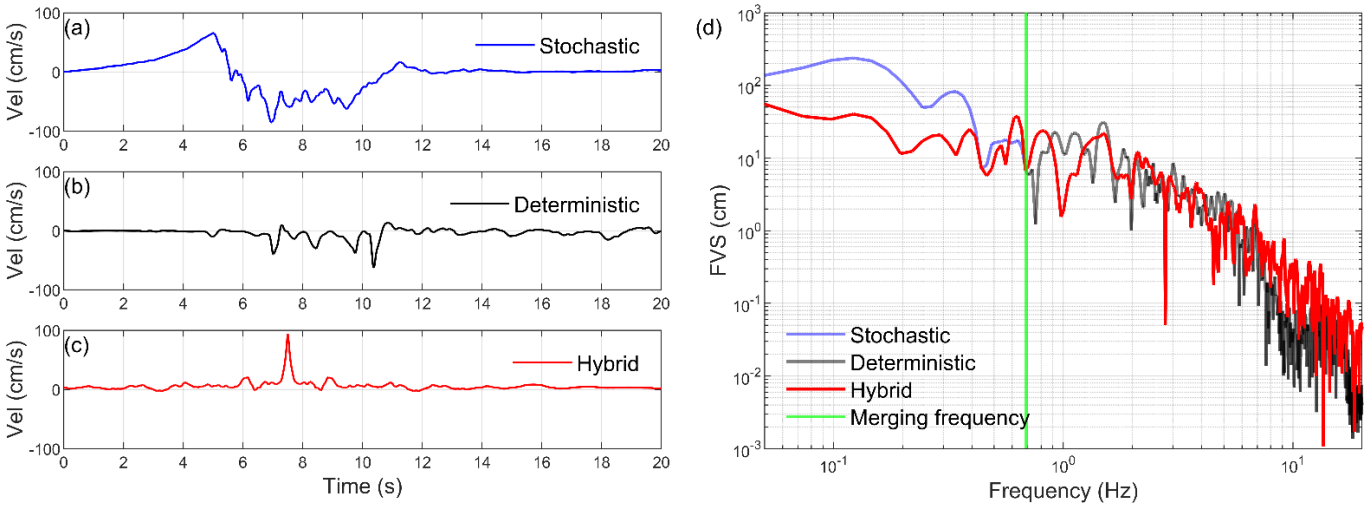

Figure 7. An example of broadband ground motion simulation realisation, with a merging frequency of 0.69 Hz.

3 Preliminary Simulation Results for the Pulse-like Waveforms

This study presents preliminary results, with further detailed work ongoing. Input parameters for the stochastic simulations are adopted from Tang et al. (2024). To enhance the reliability of the reference-rock site velocity model, we constructed it using multiple data sources. Specifically, the Vs profile is derived from the slowness model provided in Akkar and Yenier (2009), representing typical conditions in southern Türkiye. The Vp and density profile are obtained using the empirical correlation proposed by Brocher (2005). The constant Qs factor, calibrated from Tang et al. (2024) for frequencies below 1.0 Hz, is applied, and Qp is set as 2 × Qs for all layers.

Fig. 8 illustrates the constructed velocity model used in this study. The slip model applied in the simulation is sourced from Mai et al. (2023) (Fig. 9), and a detailed finite-fault model is shown in Fig. 10, including slip, rupture velocity (V_r), and rise time (T_r). Fig. 11 displays the distribution of target stations identified as producing pulse-like waveforms.

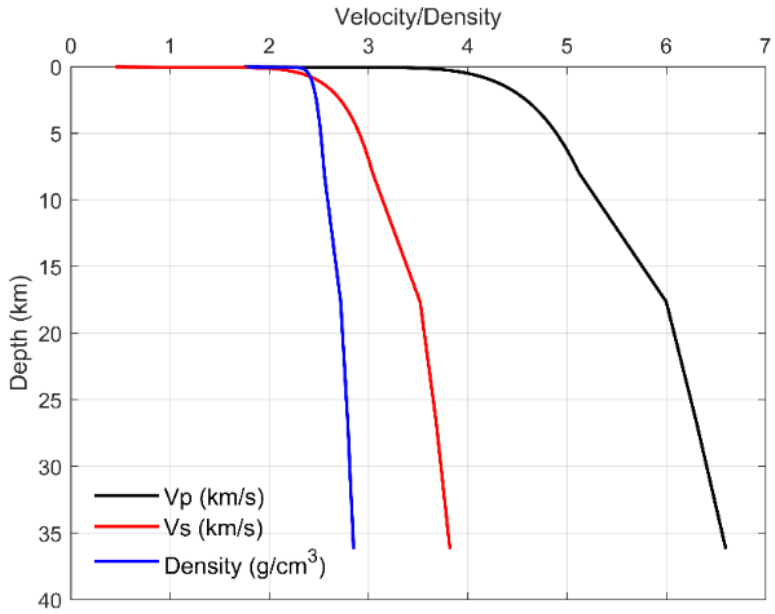

Figure 8. Velocity model used in this study.

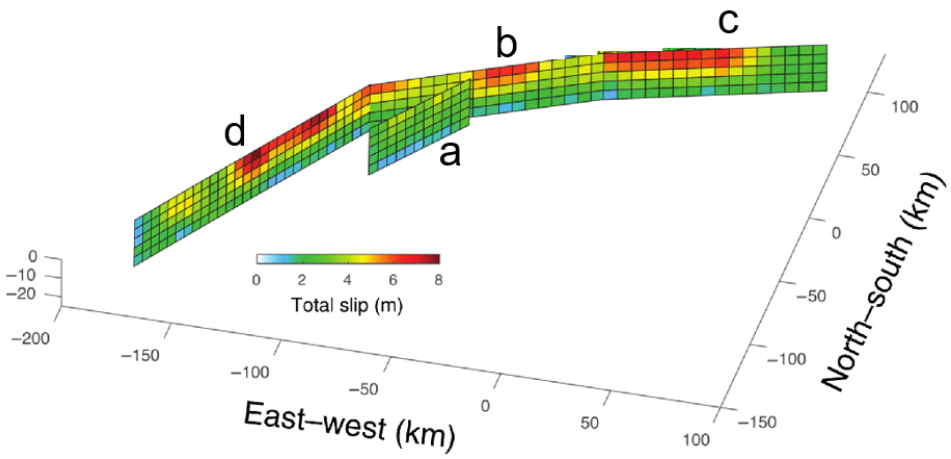

Figure 9. Slip model used in this study.

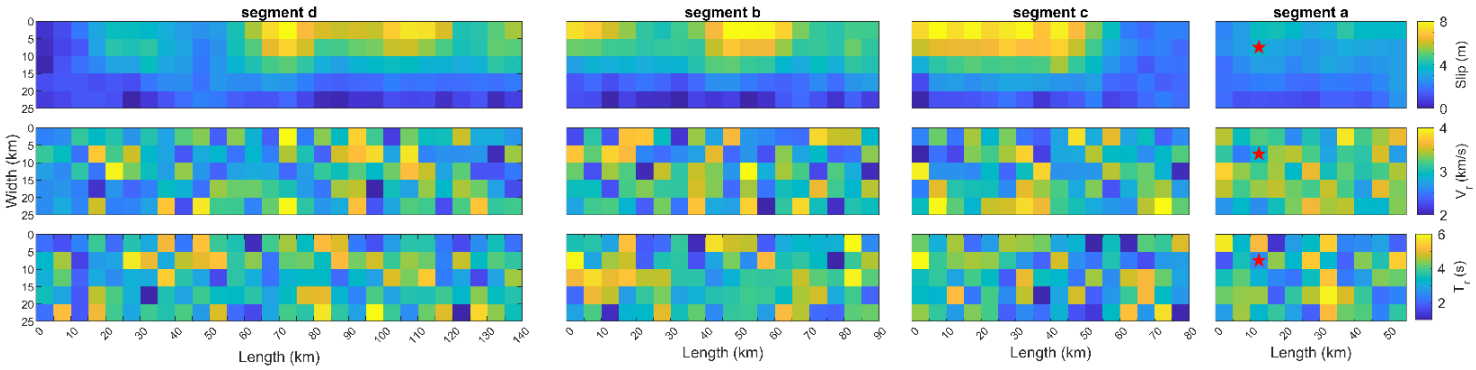

Figure 10. Detailed finite-fault model used in this study, from kinematic modelling. Details can be found in Mai et al. (2023).

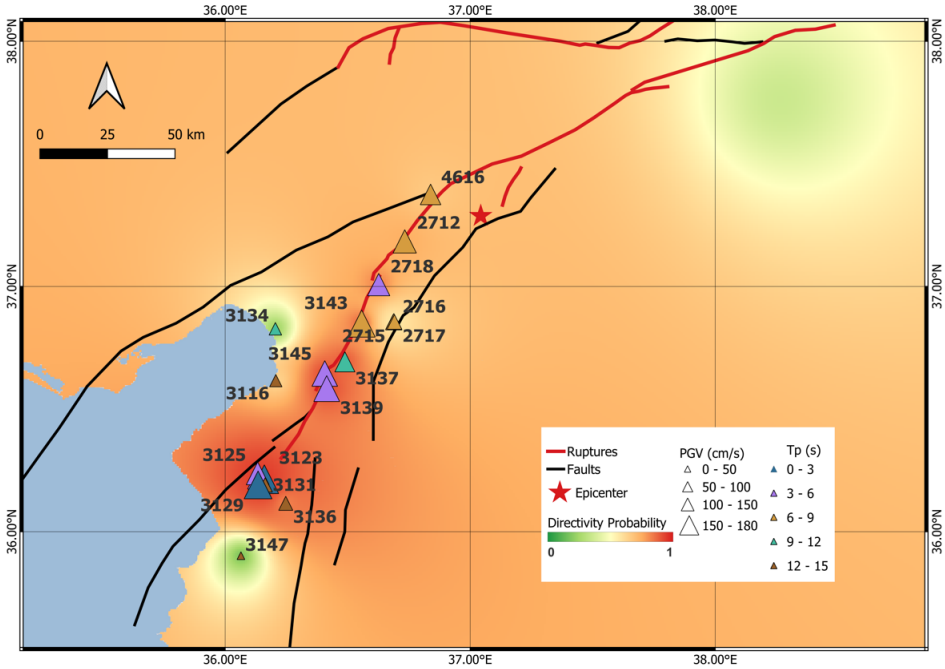

Figure 11. Distribution map of the target stations in this study. The overall colormap indicates the probability of directivity effect of the strike-slip fault; the size of the stations indicates the recorded PGV values. More information can be found in Tang et al. (2024).

In this initial study, we performed preliminary simulations, focusing solely on stochastic simulations. The recorded E-W and N-S component waveforms, alongside the simulated waveforms using a purely stochastic approach for 19 stations, are shown in Fig. 12. Fig. 13 presents both the recorded and simulated PSA, while the goodness-of-fit for these simulations is displayed in Fig. 14.

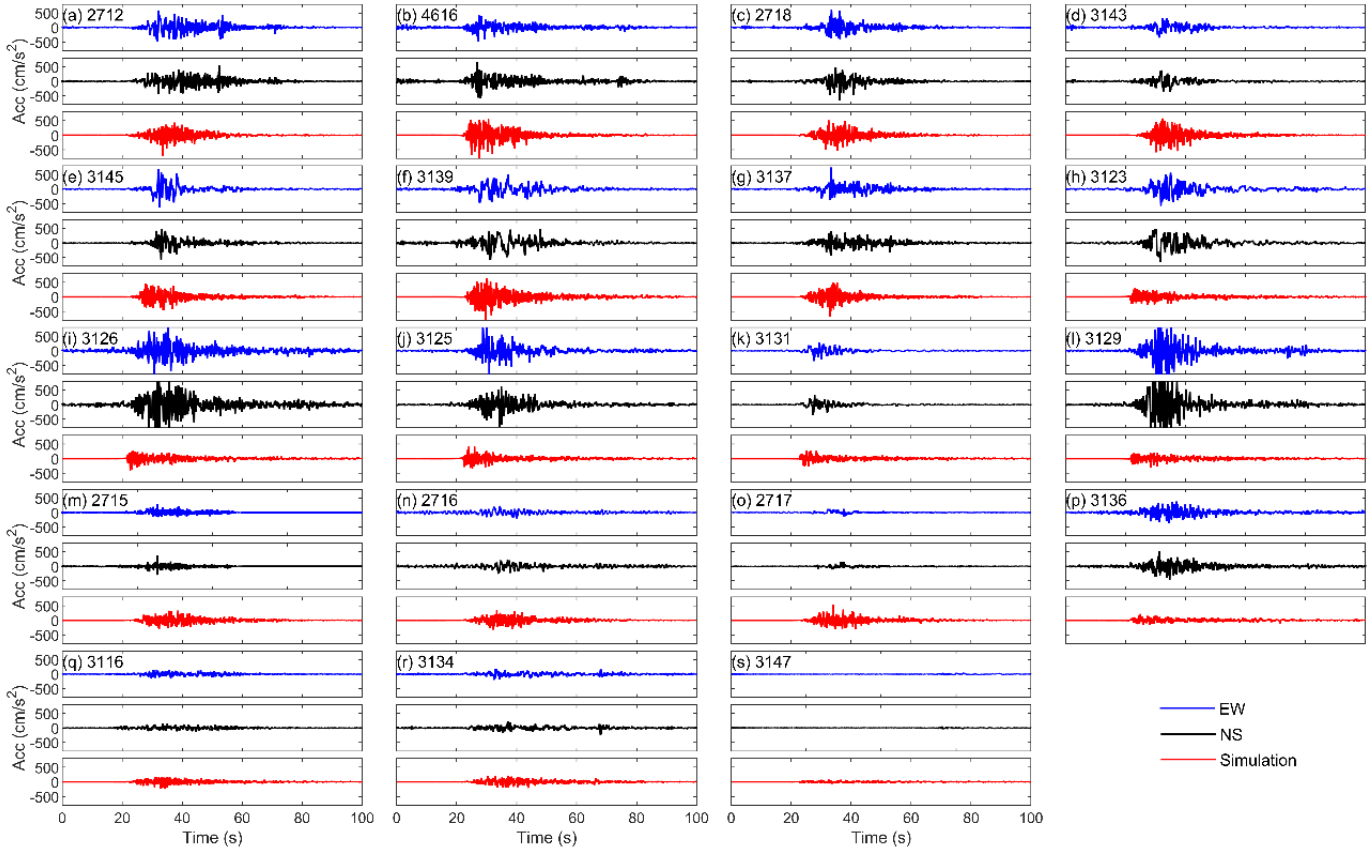

Figure 12. Recorded and simulated time series for the 19 identified stations with pulse-like waveforms.

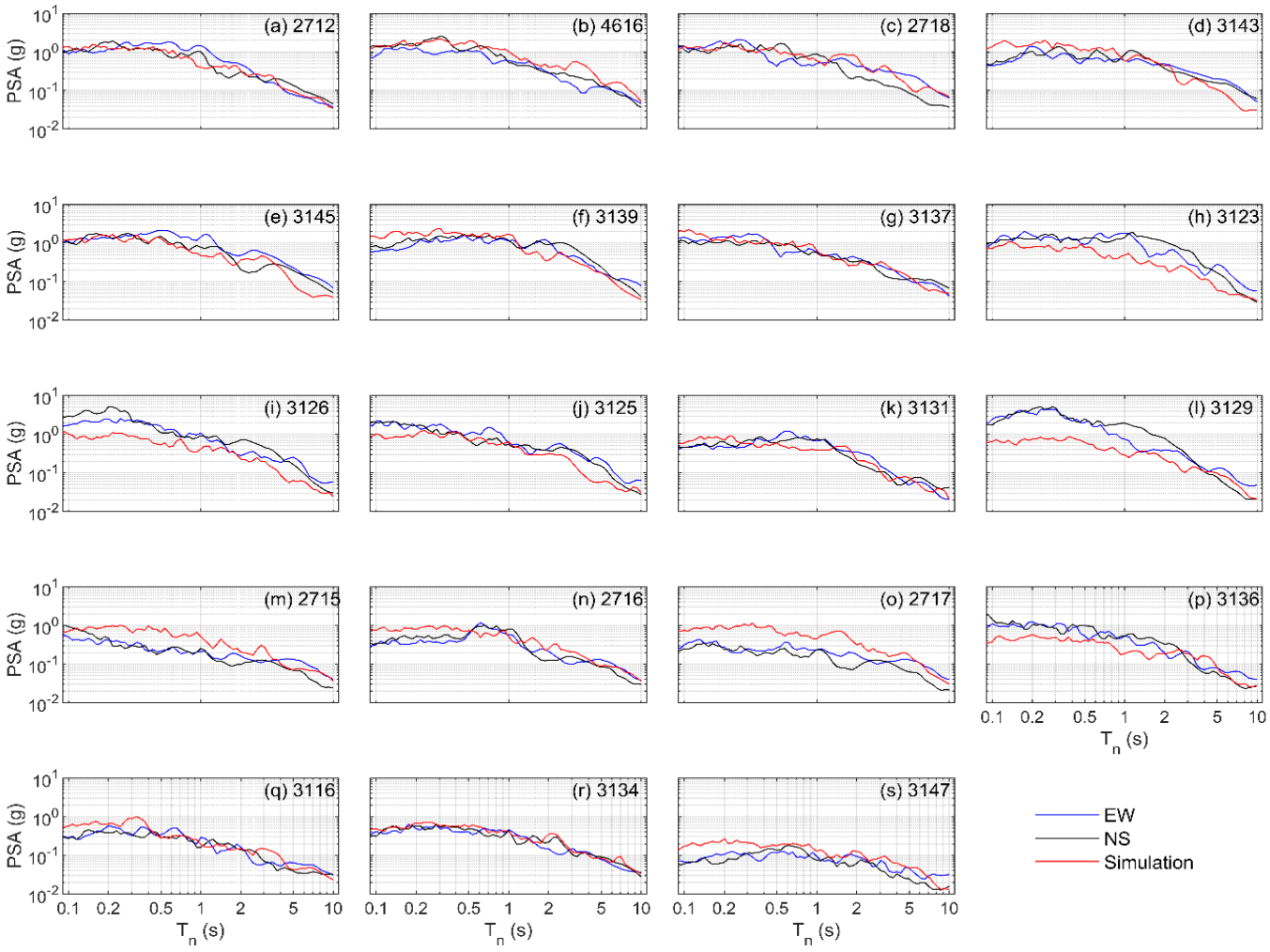

Figure 13. Recorded and simulated PSA for the 19 identified stations with pulse-like waveforms.

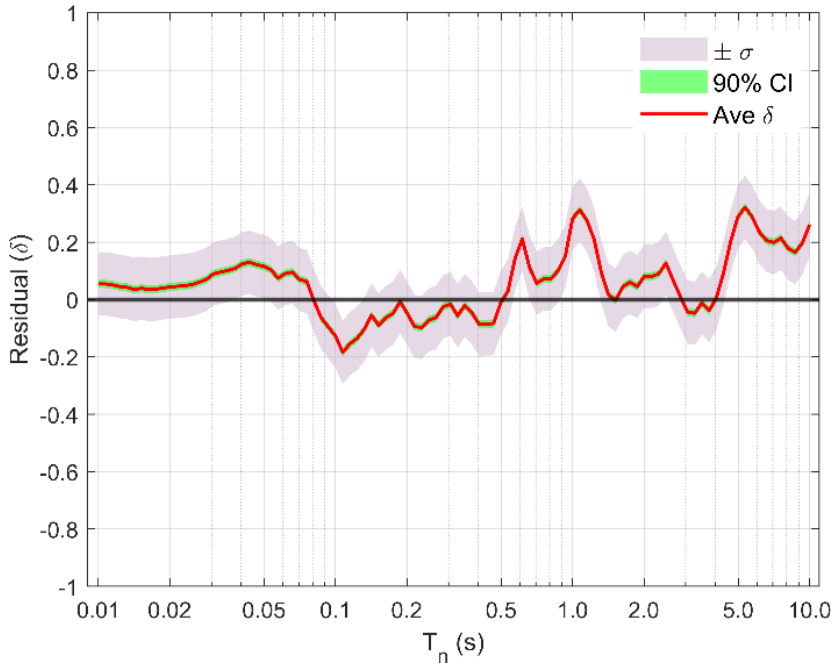

Figure 14. Residuals with respect to natural periods between 0.01 – 10.0 s, the green shaded area marks the 90% confidence interval. δ indicates the average residual, and σ represents the standard deviation. Observations are given as the RotD50 of the two horizontal components.

Figs. 12 through 14 demonstrate that our simulations generally produce intensity levels comparable to the recordings. However, the average residuals, shown in Fig. 14, indicate that the simulations tend to overestimate values at 0.01–0.07 s and periods > 0.5 s. These results highlight the need for further refinement of our simulation approach.

4 Closing Remarks

We employ a broadband ground-motion simulation approach to model the complex rupture process and wave propagation during the Mw 7.8 Pazarcık Earthquake on 6 February 2023 in Kahramanmaraş, Türkiye. Preliminary results indicate that current stochastic simulations, while able to achieve a rough match, do not capture the detailed characteristics of the ground motions.

In follow-up studies, we will conduct more in-depth simulations to address these limitations. For instance, we will examine the impact of slip distribution on ground motions by comparing uniform and kinematic slip models. Additionally, we will explore fault rupture heterogeneity by varying rupture velocity, rake angle, and rise time across subfaults. We will also quantify the radiation pattern for both low and high frequencies to assess its influence on near-field ground motions. These studies will be instrumental in refining ground motion characterizations for seismic hazard assessment.

5 References

Aki, K. and Richards, P.G. (1980). Quantitative Seismology, Theory and Methods, Freeman and Company.

Akkar S, Yenier E (2009) Assessment of point-source stochastic simulations using recently derived ground motion prediction equations, Bull. Seismol. Soc. Am., Vol 99, pp 3172–3191.

Aktug, B., Ozener, H., Dogru, A., Sabuncu, A., Turgut, B., Halicioglu, K., Yilmaz, O. and Havazli, E. (2016). Slip rates and seismic potential on the east Anatolian fault system using an improved GPS velocity field, J. Geodynam. Vol 94–95, pp 1–12.

Barka, A. (1996). Slip distribution along the North Anatolian fault associated with the large earthquakes of the period 1939 to1967, Bull. Seismol. Soc. Am. Vol 86, No. 5, pp 1238–1254.

Bayik, C., Gurbuz, G, Abdikan, ., Gormus, S. and Kutoglu, S. H. (2020). Investigation of Source Parameters of the 2020 Elazig-Sivrice Earthquake (Mw 6.8) in the East Anatolian Fault Zone. Pure Appl. Geophys., Vol 179, pp 587–598.

Boore, D. M. (2009). Comparing stochastic point-source and finite-source ground-motion simulations: SMSIM and EXSIM, Bull. Seismol. Soc. Am., Vol 99, pp 3202–3216.

Brocher, T.M. (2005). Empirical relations between elastic wave speeds and density in the Earth's crust. Bull. Seismol. Soc. Am., Vol 95, pp 2081–2092.

Bindi, D., Zaccarelli, R., Cotton, F., Weatherill, G., Kotha S. R. (2023) Source scaling and ground-motion variability along the east Anatolian fault. The Seismic Record, Vol 3, No 4, pp 311–321.

Graves, R. W. and Pitarka, A. (2010). Broadband Ground-Motion Simulation Using a Hybrid Approach, Bull. Seism. Soc. Am., Vol 100, pp 2095–2123.

Guatteri, M., Mai, P. M.and Beroza, G. C. (2005). A Pseudo-Dynamic Approximation to Dynamic Rupture Models for Strong Ground Motion Prediction, Bull. Seismol. Soc. Am., Vol 94, No 6, pp 2051–2063.

Haskell, N. A. (1953). The dispersion of surface waves on multilayered media, Bull. Seismol. Soc. Am., Vol 43, pp 17–34.

Haskell, N. A. (1964). Radiation pattern of surface waves from point sources in a multi-layered medium, Bull. Seismol. Soc. Am., Vol 54, pp 377–393.

Mai, P. M. and Beroza, G. C. (2002). A spatial random field model to characterize complexity in earthquake slip, J. Geophys. Res., Vol 107, No B11, pp 2308.

Mai, P. M., Imperatori, W. and Olsen, K. B. (2010). Hybrid broadband ground-motion simulations: Combining long-period deterministic synthetics with high-frequency multiple S-to-S backscattering, Bull. Seismol. Soc. Am., Vol 101, pp 2124–2142.

Mai, P. M., Spudich, P. and Boatwright, J. (2005). Hypocenter Locations in Finite-Source Rupture Models. Bull. Seismol. Soc. Am., Vol 95, No 3, pp 965–980.

Mai, P. M. and Thingbaijam, K. K. S. (2014). SRCMOD: An Online Database of FiniteFault Rupture Models, Seismol. Res. Letts. Vol 85, No 6, pp 1348-1357.

Mai, P. M., Aspiotis, T., Aquib, T. A., Cano, E. V., Castro-Cruz, D., Espindola-Carmona, A., Li, B., Li, X., Liu, J., Matrau, R. et al. (2023). The Destructive Earthquake Doublet of 6 February 2023 in South-Central Türkiye and Northwestern Syria: Initial Observations and Analyses, The Seismic Record, Vol 3, No 2, pp 105–115.

Motazedian, D. and Atkinson, G. M. (2005). Stochastic finite-fault modeling based on a dynamic corner frequency, Bull. Seismol. Soc. Am., Vol 95, pp 995–1010.

Miyake, H., Iwata, T. and Irikura, K. (2003). Source Characterization for Broadband Ground-Motion Simulation: Kinematic Heterogeneous Source Model and Strong Motion Generation Area, Bull. Seismol. Soc. Am., Vol 93, No 6, pp 2531–2545.

Pousse-Beltran, L., Nissen, E., Bergman, E. A., Cambaz, M. D., Gaudreau, É., Karasözen, E., Tan, F. (2020). The 2020 Mw 6.8 Elazığ (Turkey) earthquake reveals rupture behavior of the East Anatolian Fault, Geophys. Res. Lett., Vol 47, pp 1–14.

Pulido, N. and Dalguer, L. A. (2009). Estimation of the High-Frequency Radiation of the 2000 Tottori (Japan) Earthquake Based on a Dynamic Model of Fault Rupture: Application to the Strong Ground Motion Simulation, Bull. Seismol. Soc. Am., Vol 99, No 4, pp 2305–2322.

Şeşetyan, K., Demircioğlu, M. B., Duman, T., Çan, T., Tekin, S., Eroğlu, A. TZülfikar, Ö. (2018). A probabilistic seismic hazard assessment for the Turkish territory part I: The area source model, Bull. Earthq. Eng., Vol 16, pp 3367–3397,

Tang, Y. (2022a). An Updated Corner-Frequency Model for Stochastic Finite-Fault Ground-Motion Simulation, Bull. Seismol. Soc. Am., Vol 112, pp 921–938.

Tang, Y. (2022b). GMSS2.0: An Enhanced Software Program for Stochastic Finite-Fault Ground-Motion Simulation, Seismol. Res. Lett., Vol 93, pp 1868–1879.

Tang, Y., Şeşetyan, K., Mai, P. M. (2024). Comprehensive ground-motion characterization of the 6 February 2023 MW 7.8 Pazarcık earthquake in Kahramanmaraş, Türkiye: insights into attenuation effects, site responses and source properties, Bull. Earthquake Eng., https://doi.org/10.1007/s10518-024-02028-2.

Thomson, W.T. (1950). Transmission of elastic waves through a stratified solid medium, J. Appl. Phys., Vol 21, pp 89–93.

Tinti, E., Fukuyama, E., Piatanesi, A. and Cocco, M. (2005). A Kinematic Source-Time Function Compatible with Earthquake Dynamics, Bull. Seismol. Soc. Am., Vol 95, No 4, pp 1211–1223.

Zhu, L. and Rivera, L. A. (2002). A note on the dynamic and static displacements from a point source in multilayered media, Geophys. J. Int., Vol 148, pp 619–627.